COMBUSTION SCIENCE AND TECHNOLOGY
2017, VOL. 189, NO. 9, 1551–1570
https://doi.org/10.1080/00102202.2017.1308357

Taylor & Francis
Taylor & Francis Group



# Physics-Based Modeling of Live Wildland Fuel Ignition Experiments in the Forced Ignition and Flame Spread Test Apparatus

C. Anand[a], B. Shotorban[a], S. Mahalingam[a], S. McAllister[b], and D. R. Weise [c]

[a]Department of Mechanical and Aerospace Engineering, The University of Alabama in Huntsville, Huntsville, Alabama, USA; [b]Rocky Mountain Research Station, USDA Forest Service, Missoula, Montana, USA; [c]Pacific Southwest Research Station, USDA Forest Service, Riverside, California, USA

**ABSTRACT**

A computational study was performed to improve our understanding of the ignition of live fuel in the forced ignition and flame spread test apparatus, a setup where the impact of the heating mode is investigated by subjecting the fuel to forced convection and radiation. An improvement was first made in the physics-based model WFDS where the fuel is treated as fixed thermally thin elements and then it was utilized in this study. This improvement included bound water in addition to free water in fuel moisture content. The fuel was assumed to undergo evaporation of free and bound water, pyrolysis and char oxidation. Fuels with different moisture contents ranging from 0% to 130% were simulated under an identical heating condition. The simulated and the experimental ignition times compared reasonably well with each other. The time evolutions of simulated and experimental mass loss rates also compared well with each other. For all fuel moisture contents, it was observed that the release of bound moisture starts at temperatures greater than 200°C long after ignition time. This observation was consistent with the release of moisture observed at high temperatures in the experiments of live fuels.

**ARTICLE HISTORY**
Received 9 August 2016
Revised 8 March 2017
Accepted 15 March 2017

**KEYWORDS**
Live fuels; Piloted ignition; Pinus; *Pseudotsuga*; Wildland fire

## Introduction

In wildland fires, the fuel moisture content (FMC), defined as the ratio of water mass to dry mass of fuel plays an important role in determining the time to ignition. Live fuels have moisture contents much larger than 100% of their oven dry weight (Weise et al., 2005). Owing to the differences in chemical composition and how water is stored in live and dead fuels, live fuels burn at fuel moisture contents where dead fuels do not. The moisture of extinction for dead fuels is often found to be in the range 30–70% FMC, whereas experiments based on the burning of live fuels (McAllister et al., 2012; Pickett et al., 2010; Xanthopoulos and Wakimoto, 1993) show that live fuels can sustain fire spread for FMC beyond the range prescribed for dead fuels. The most unpredictable fires often occur in crowns of vegetation composed of live fuel

**CONTACT** Babak Shotorban babak.shotorban@uah.edu Department of Mechanical and Aerospace Engineering, The University of Alabama, 301 Sparkman Drive, Huntsville, AL 35899, USA.

Color versions of one or more of the figures in the article can be found online at www.tandfonline.com/gcst.

elements. These crown fires are uncontrollable and have a higher spread rate compared to surface fires (Rothermel, 1972).

To understand the burning behavior of live fuels and examine the relationship between FMC and ignition time, piloted ignition experiments of cellulosic materials were performed and correlations between moisture content and ignition times were deduced (Atreya and Abu-Zaid, 1991; Moghtaderi and Fletcher, 1988; Simms and Law, 1967). Woody materials were used as fuel and it was found that moisture increased the energy required for ignition, resulting in a delayed ignition time. Ignition time was correlated with moisture content and material properties of wood, such as emissivity, thermal conductivity, and density. FMC in live fuels exhibited diurnal and seasonal variation during which both dry and moist weight of the fuels vary (Blackmarr and Flanner, 1968; Jameson, 1966; Philpot, 1965; Van Wagner, 1967). Experiments conducted by Dimitrakopoulos and Papaioannou (2001), McAllister et al. (2012), Pellizzaro et al. (2007), Pickett et al. (2010), Smith (2005), Weise et al. (2015), and Xanthopoulos and Wakimoto (1993) used live fuels wherein the fuel moisture content evolved naturally over the course of an annual season. Species specific empirical correlations relating ignition time to moisture content for various live vegetation species were established. McAllister et al. (2012) performed piloted ignition experiments using the forced ignition and flame spread test (FIST) apparatus on live fuels, such as Douglas-fir (*Pseudotsuga menziesii*) and lodgepole pine (*Pinus contorta*). These fuels were collected throughout the growing season, thereby the natural variation in moisture content and chemical composition was factored in. These two species behaved as thermally intermediate materials with the existence of temperature gradients within the needles during pyrolysis. McAllister et al. (2012) suggested that the extremely vigorous fires observed in high moisture content live fuels could be due to the different physical mechanisms through which water is stored, causing it to evaporate at different rates. It was also observed that when live fuels were heated, the needles underwent a structural failure resulting in the release of water in an explosive process unlike in dead fuels, wherein water was released through evaporation alone. Ignition times differed for fuels with identical FMCs that were tested during different seasons, in all likelihood, due to the structural changes that occur in these fuels (Fletcher et al., 2007; Jolly et al., 2012; Killebrew, 1878; Kozlowski and Clausen, 1965; Little, 1970).

Since evaporation of water is an endothermic reaction, fuel moisture content affects heat transfer and combustion processes in both solid and gas phases hence delaying the time to ignition. In the solid phase, moisture affects thermal properties, such as density, thermal conductivity, and specific heat, whereas in the gas phase water vapor dilutes flammable pyrolysates and absorbs energy (Albini, 1980; Finney et al., 2013). The modeling of a wildland fire by Albini (1980) and the modeling of premixed and non-premixed flames by Ferguson et al. (2013) showed significant impact of fuel moisture on the flame. While some studies (Babrauskas, 2003; McAllister et al., 2012; Prince and Fletcher, 2013) reported the simultaneous evolution of water vapor and pyrolysis gases during ignition, most numerical models for solid fuel degradation considered a sequential process of evolution of water vapor and pyrolysis gases wherein water is assumed to evaporate first (at temperatures close to 100°C), followed by the pyrolysis gas release.

An important parameter, which describes the storage of water, is the fiber saturation point (FSP). FSP is the point in the drying process at which only water bound in the cell

walls remains and all other water, called free water, has been removed from the cell cavities. Below FSP, the wood cell shrinks and changes physically. FSP for wood lies in the range of 23–30% (Jolly et al., 2014; Ross, 2010) on a dry weight basis. Previous experiments on live fuels (Gallacher, 2016; Nelson, 2001; Pickett et al., 2010) have suggested that free water is released at temperatures close to the boiling point of water while bound water and pyrolysis gases vaporize at temperatures greater than 200°C. Hence, it is important to include these effects in the modeling of moisture in live fuels. Prince (2014) and Prince and Fletcher (2013) conducted ignition experiments on manzanita leaves and developed evaporation models differentiating live and dead fuels. This work emphasized modeling bound water in live fuels, which accounted for the release of moisture in the temperature range 266–315°C. The models showed a good agreement between predicted and experimental mass loss. Using Arrhenius parameters for bound water, Prince and Fletcher (2013) and Yashwanth et al. (2015) performed physics-based modeling to study the effect of heating modes and moisture content on ignition of manzanita leaves and found the predicted ignition and burnout time to be consistent with experimental results.

The aim of the present study is to improve the understanding of ignition and combustion of live foliage based on the recent experiments of McAllister et al. (2012). Here, Wildland-urban interface fire dynamics simulator (WFDS SVN9977) (McGrattan et al., 2008; Mell et al., 2009), in which solid fuels are represented by discrete particles, was used for computations. The input file used for WFDS is given in the Appendix. Since the current version of WFDS does not differentiate between bound and free water in fuel, bound and free water was modeled via Arrhenius rate equations in the solid fuel thermal degradation module. Hence, the fuel was assumed to undergo a three-stage decomposition process, consisting of evaporation of bound and free water, pyrolysis, and char oxidation. The pyrolyzate gas was assumed to be methane that reacted with air through a single-step mixing-controlled chemical reaction.

## Numerical model and computational setup

The experimental setup of McAllister et al. (2012) is replicated by WFDS, which solves the three-dimensional time dependent equations for low Mach number flows with combustion and heat transfer. The large eddy simulation (LES) with Deardorff's model (Deardorff, 1980) for subgrid-scale terms is utilized to deal with turbulence. To calculate thermal radiation, a radiation transport equation is solved with a non-scattering gray gas assumption. The solid phase is modeled as discrete particles fixed in space. Particles are assumed thermally thin and optically black fuel elements. The convective and radiative heat transfer between the gas phase and solid vegetation particles is assumed present. The solid fuel particles experience mass loss with an increase in temperature. As the temperature of the fuel increases, free water, bound water, and pyrolysis gas release and finally char oxidation takes place. The solid phase degradation model for solid fuel is based on the Arrhenius rate equation:

$$\dot{m}_i''' = -m_i''' A_i \exp\left(\frac{-E_i}{RT_{\text{veg}}}\right) \tag{1}$$

where $m_i'''$ represents mass per unit volume, $\dot{m}_i'''$ is the mass loss rate per unit volume, $A_i$ is the pre-exponential factor, $T_{\text{veg}}$ represents the vegetation temperature, $R$ is the universal

**Table 1.** Thermokinetic parameters for solid fuel degradation.

| | $A_i$ ($s^{-1}$) | $T_i$ (K) |
|---|---|---|
| Free water | $5.13\times10^{10}$ | 10584 |
| Bound water | $3.0\times10^{13}$ | 18000 |
| Pyrolysis gas | $3.63\times10^{4}$ | 7250 |

gas constant, and $E_i$ is the activation energy. Here, $i$ is a generic index used for the species free water, bound water, and dry fuel. In Table 1, $A_i$ and the activation temperature, defined by $T_i = E_i/R$, are tabulated for three species.

To model the volatilization process, by default, WFDS uses thermokinetic constants available for pine needle combustion (Grishin, 1997; Porterie et al., 2005). The same constants are used for Douglas-fir needles here since the thermokinetic constant values are unknown for Douglas-fir needles. This seems to be a reasonable approximation given that both species belong to the *Pinaceae* family of species. A similar approximation was also made by Mell et al. (2009). The thermokinetic constants of bound and free water used here were compiled from the works of Bryden et al. (2002), Chan et al. (1985), Prince and Fletcher (2013), and Yashwanth et al. (2015). It is noted that the species-specific thermokinetic constants for bound water was based on the experiments conducted on manzanita leaves with a suggested activation temperature of 20000 K (Prince and Fletcher, 2013). A sensitivity analysis on the activation temperature of bound water was performed and it was observed that changing the activation temperature by 10% resulted in less than 1% change in the results (such as peak mass loss rate and heat release rate). The energy equation for the fuel is:

$$\rho c_p \frac{dT_{\text{veg}}}{dt} = -\Delta h_{\text{vap}} \dot{m}'''_{\text{free}} - \Delta h_{\text{vap}} \dot{m}'''_{\text{bound}} - \Delta h_{\text{pyr}} \dot{m}'''_{\text{pyr}} - \nabla \cdot \mathbf{q}_c - \nabla \cdot \mathbf{q}_r \tag{2}$$

where the first three terms on the right–hand side represent the energy release due to the evaporation of free and bound water, and release of pyrolysis gases, respectively. Here, $\Delta h_{\text{vap}}$ represents the enthalpy of moisture vaporization set equal to 2259 kJ/kg (Mell et al., 2009), which is used for both free and bound water here, and $\Delta h_{\text{pyr}}$ is the enthalpy of volatilization set equal to 418 kJ/kg (Mell et al., 2009). In Eq. (2), $\mathbf{q}_c$ and $\mathbf{q}_r$ denote convective and radiative heat fluxes, respectively, to the bulk of fuel.

The computational domain resembled the FIST apparatus displayed in Figure 1 (McAllister et al., 2012). It consisted of a small wind tunnel, infrared heater, coiled wire ignitor, and a high precision mass balance. The Douglas-fir needles were placed on a sample holder located on the mass balance and were heated from above by an infrared heater producing a uniform heat flux of 50 $kW/m^2$ at its surface. An airflow over the sample pushed the pyrolysis gases from the heated sample over an ignitor placed at a downstream location. In the experiments, since the radiant heater alone was insufficient to achieve ignition, the ignitor was held at a temperature above 1000°C, thereby heating the gas phase and initiating ignition. These values approximate the high heat fluxes associated with a wildfire.

Shown in Figure 2 is the computational domain with dimensions 60 × 26 × 10.5 cm (L × W × H) in $x$, $y$, and $z$ directions, respectively. These dimensions were consistent with the actual dimensions of the midsection of the wind tunnel where experiments were carried out. The body of the wind tunnel used in the experiments was made of aluminum 6160 and painted on the inside with high temperature flat black stove paint. The floor of the wind tunnel

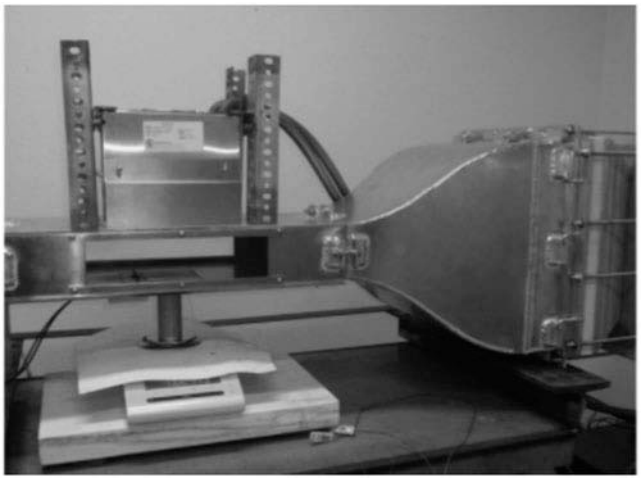

**Figure 1.** Forced ignition and flame spread test (FIST) apparatus used in McAllister et al. (2012).

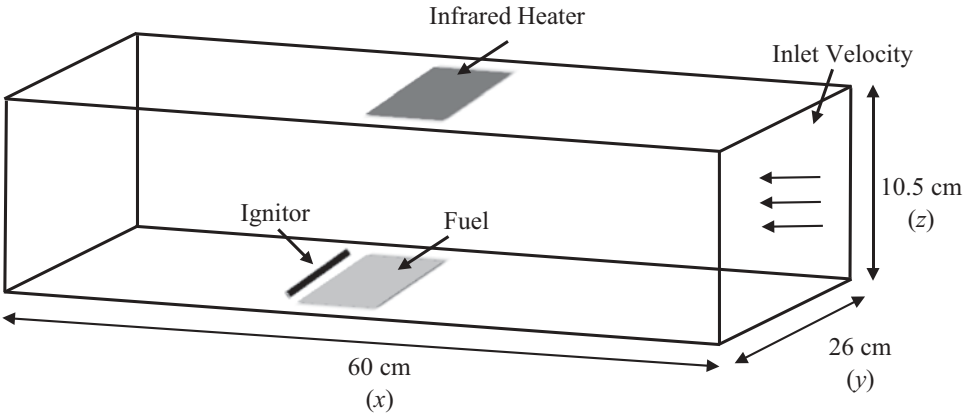


**Figure 2.** Computational domain of the wind tunnel setup used in the FIST apparatus. Fuel is uniformly distributed in a 9 cm × 9 cm rectangular region.

had a thickness of $3/8''$ and a layer of mica of thickness $1/4''$. Also, it was observed that the fire was located at a distance close to 10 cm away from the walls of the wind tunnel. Considering the material properties, proximity of the fire to the walls and the occurence of ignition in a time period of about 40 s, the walls were assumed to have minimal heating effect on the results. Hence, the walls of the wind tunnel were modeled to be inert and maintained at an ambient temperature of 293 K. A velocity inlet boundary condition at the right entrance of the wind tunnel established a laminar airflow with a velocity of 1 m/s and an open boundary condition was specified at the left exit. The Douglas-fir needles, with an initial total mass of 4 g, were approximated as fixed, thermally-thin fuel elements with homogeneous composition and uniform distribution within a rectangular region with dimensions similar to the sample holder (9 cm in length and 9 cm in width) used in experiments. The vegetative dry and moist mass was also uniformly distributed among all fuel elements. The infrared heater was modeled as a 9×9 cm surface maintained at a temperature of 971 K, thereby producing a heat flux of

50 kW/m$^2$ at the surface of the heater. A few non-reacting fuel particles held at a constant temperature of 1500°C modeled the ignitor, located at a distance 1.2 cm downstream of the fuel elements, centered 6 mm off the bottom. It is noted that McAllister et al. (2012) mentioned the ignitor temperature was above 1000°C without giving an exact value for the ignitor temperature.

Ignition criteria is commonly defined as the time taken by the solid fuel to reach a specific ignition temperature. Based on experiments on live fuel burns (Janssens, 1991; Smith, 2005; Xanthopoulos and Wakimoto, 1993) it is found that the ignition temperature for live fuels lies in the range 300–355°C. It is also noted that the ignition temperature varies with the fuel moisture content and is often dependent on the experimental setup. Here, we defined time to ignition as the time at which the global heat release rate reaches one half of its initial peak value. Since the peak value of heat release rate varies as a function of FMC, the ignition criteria varies with FMC as well. Based on the range of FMC observed over different seasons in the experiments, a range of 0% (dry fuel) and 70–130% was considered. Two types of model were considered for water: one assumed water at a free state only and the other included bound water in addition to free water. The initial mass distribution of free and bound water was determined by the FSP. Since the FSP of the investigated Douglas-fir needles was unknown, the FSP of wood, equivalent to 30% of FMC (Ross, 2010) is considered. Accordingly, for FMC ranging from 70–130%, the bound water mass decreased from 0.71 g to 0.52 g, while the initial free water mass increased from 0.95 g to 1.74 g. A total of nine simulations were performed. Four simulations considered FMC in the range of 70–130% for each water model type and one simulation with no moisture, representing dry fuel. A uniform grid size of 5 mm was used in all simulations. In this work, LES is used to model turbulence wherein the filter size is set identical to the grid size. Hence, subgrid-scale terms, which are a function of the filter size, and subsequently the filtered gas phase equations, which include subgrid-scale terms, change with the change in grid size (Pope, 2004). Thus, a grid dependency study, as it is practiced in simulations of laminar flows or direct numerical simulations of turbulent flows, is inadequate. We have conducted the simulations with the highest possible resolution. Furthermore, to test the adequacy of the resolution, we used a criterion based on the characteristic flame diameter ($D^*$). Although this test was suggested for buoyant plumes, it was also used for wind tunnel scenarios and compartmental fires (Overholt et al., 2014; Wang et al., 2016). For a uniform grid size ($\Delta x$) of 5 mm and for the range of moisture contents studied, the ratio of $D^*/\Delta x$ was found to vary in the range of 13.2 to 16.0. It has been noted from previous studies (Dreisbach and Hill, 2007; Overholt et al., 2014; Wang et al., 2016) that this ratio must be in the range between 4 and 16 to obtain results adequate for engineering calculations. All simulations were performed for a burning time of 250 s, using 40 processors of the dense memory cluster at the Alabama Supercomputing Center.

## Results and discussion

Figure 3 shows the ignition time versus FMC. For all moisture contents, it was found that by including the effect of bound water, ignition occurred around 5 s prior to that observed in the cases where moisture was regarded as free water only. The ignition times obtained from the experiments had an uncertainty of about 2.5 s. For the free

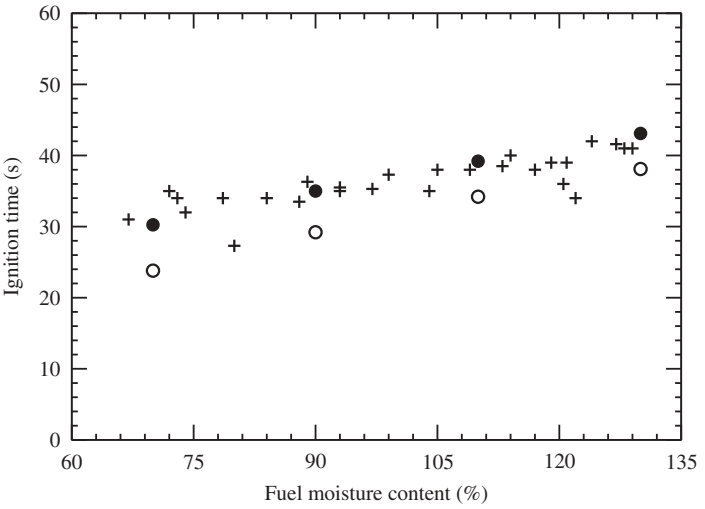


**Figure 3.** Variation of ignition time against fuel moisture content in experiments (+); modeling with FMC in the free only state (•); and modeling with FMC in the free and bound states (○).

water only case, the simulated ignition times were found to lie within the observed uncertainty in experimental measurements for all moisture contents. For the free and bound water case, at 70% FMC, there was a difference of around 5 s between the simulated and experimental ignition times (considering the uncertainty of 2.5 s). However, for higher moisture contents (to 130% FMC), this difference is lower and the simulated ignition times laid within the uncertainty of the experimental values. The reason for delayed ignition in the free water only case can be attributed to the fact that ignition was only observed after a significant amount of moisture was released from the fuel at temperatures close to 100°C. Since evaporation of water is an endothermic process, a significant increase in fuel temperature is inhibited during this process thereby delaying the process of volatilization and hence ignition. On the other hand, when the effect of bound water was included, a part of the moisture was released at temperatures close to 100°C and the rest was released only after the solid fuel attained temperatures close to 200°C. The process of volatilization began prior to the release time of bound water, thereby resulting in the release of pyrolysis gases and initiation of ignition relatively earlier. For dry fuel, the experimental and simulated time to ignition was 9 s and 10 s, respectively. A linear regression was conducted on the experimental data displayed in Figure 3 and the experimental data available for the dry fuel to find a correlation between the ignition time and FMC (McAllister et al., 2012). The regression equation was found to be $t_{ig} = 0.266 \times \text{FMC} + 8.83$ for the experimental data. A linear regression was also performed for the modeling data where moisture content was assumed to be in both free and bound water states, as shown in Figure 3, and the modeling data for dry fuel. The regression equation was $t_{ig} = 0.2185 \times \text{FMC} + 9.58$ for the modeling data. The slopes in these two correlations compared well with each other. The deviation between the simulated and experimental values could have two reasons: (1) It was found in the experiments (McAllister et al., 2012) that the fuels that were harvested at different seasons but had an identical FMC

showed different ignition times; (2) It was also found in the experiments of McAllister et al. (2012) that, in addition to the process of evaporation, an explosive process of rupturing of the heated vegetation cell walls contributed to the release of moisture. As a result of this explosion, it was speculated that some of the volatiles were also released with water. In the modeling study, neither the effect of season nor the phenomena of explosion was taken into account.

Figure 4 shows the temporal evolution of the total fuel mass. The experiments were performed thrice every week during the growing season from March–October. Because of

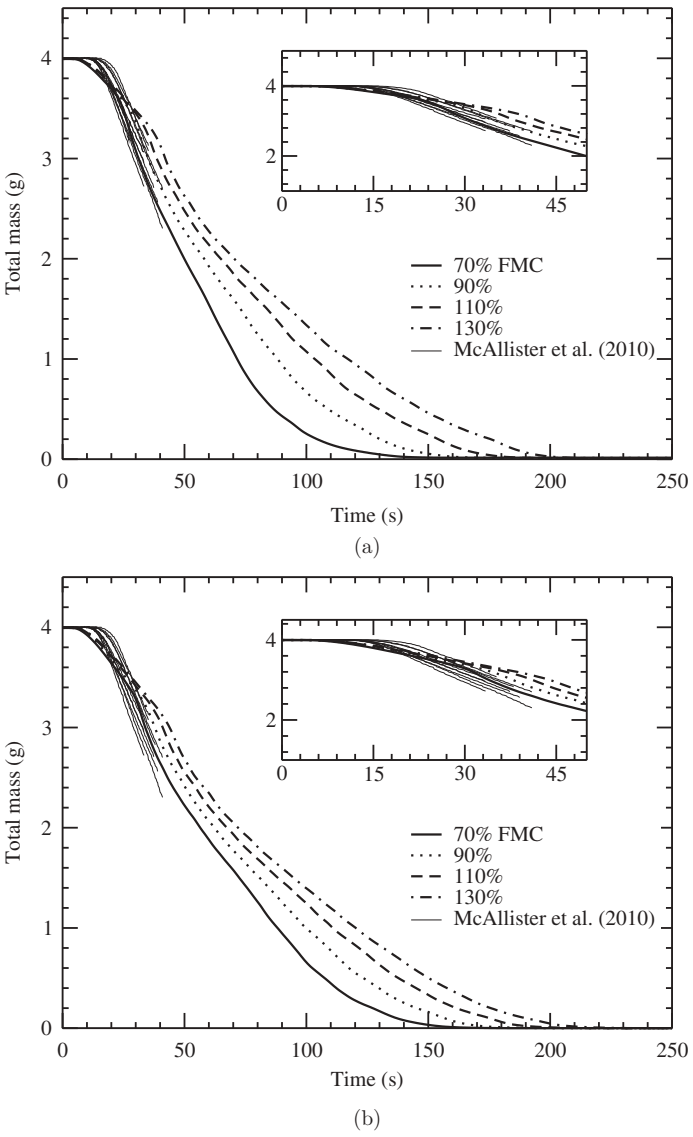


**Figure 4.** Variation of total mass of the fuel with time in modeling (lines) and experiments (thin lines) for fuels with moisture content ranging from 70–130%: (a) free and bound water case and (b) free water only case. The inserted panel shows comparsion between modeling and experimental data up to $t$ = 50 s.

seasonal changes, the FMC was different each week. The experimental data in Figure 4 and 5 was obtained by burning 12 samples, each harvested in a different week, with FMCs ranging from 70% to 130%. The burning measurement of each sample was terminated soon after flaming ignition was observed in the gas phase. On the other hand, the simulations were performed until the fuel was completely burned. Depending on the initial fuel moisture content, the burning time varied from 150 s to 200 s. It was observed in both experiments and simulations that the fuel mass loss was insignificant up to around 10 s. After this time, the temperature of the fuel element increased to values larger than the boiling point of water and the processes of evaporation and devolatilization became significant; hence, the curves dropped rapidly. At 200 s, the volatiles and moisture were completely released, leaving behind char which underwent oxidation. Comparing inset plots in Figures 4a and 4b reveals that, in the beginning, mass loss occurs slower in panel (b) than panel (a). This slower mass loss occurs because the free water evaporation is completed sooner in (a) than in (b), as there is more free water to be evaporated in the free water only case than in the free and bound water case. Overall, simulations better compare against experiments for the mass loss when water is treated in both free and bound states.

In Figure 5, time histories of the total mass loss rate of the fuel for various FMCs are displayed. It was observed that the peak value of mass loss rate decreased with an increase in FMC. The peak mass loss rate for all moisture contents occured well after ignition was observed, between times 30–50 s. The case with FMC of 70% had a maximum peak at 0.084 g/s.

In order to gain a better insight into evaporation of fuel moisture, mass loss rates of free and bound water are plotted against time in Figure 6. As the temperature of the fuel element increased close to the boiling point of water, free water was first released. Figure 6a shows the peak mass loss rate of free water increased with an increase in moisture content and the maximum peak was observed for moisture content 130% at 0.0275 g/s occurring at time 28 s. Also, it was observed that free water was completely

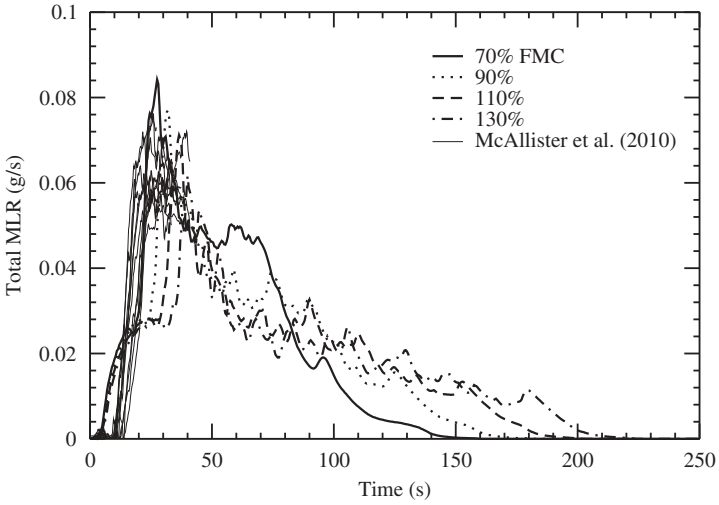


**Figure 5.** Variation of total mass loss rate with time in modeling (lines) and experiments (thin lines) for fuels with moisture content ranging from 70–130%.

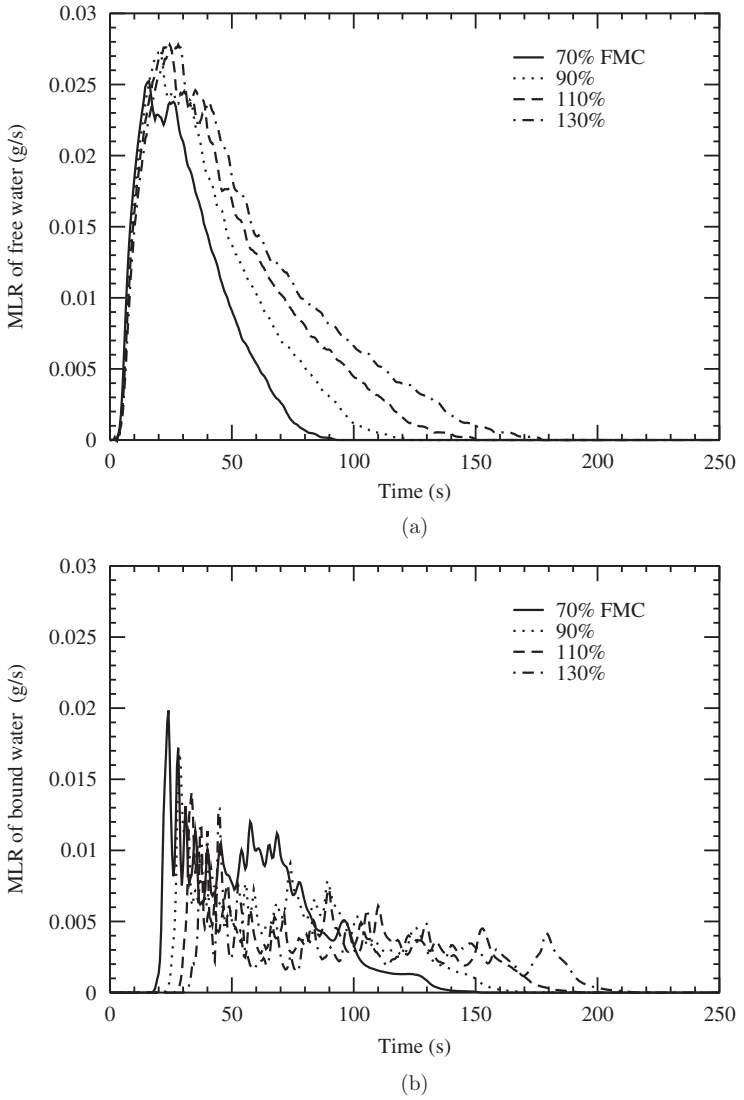


**Figure 6.** Variation of fuel moisture mass loss rate with time: (a) free water and (b) bound water.

released before 75 s in all cases. On the other hand, the initiation of bound water evaporation was observed at a later time around 15 s after free water evaporation was initialized, seen in Figure 6b. Here, the fuel elements attained temperatures greater than 200°C. For all moisture contents, it was observed that the peak mass loss rate of bound water occurs close to the time of ignition. It is noted that bound water was released simultaneously with the fuel volatiles and the evaporation of bound water was completed almost 60 s after the evaporation of free water was completed. Also, for larger FMCs, the ratio of bound water mass to free water mass is smaller given that the total mass of fuel is identical in all modeling cases. Hence, unlike free water, it was observed here that the peak mass loss rate of bound water decreased with an increase in moisture content. This peak occurred approximately 15 s after the peak mass loss rate of free water did. The

peak mass loss rates (MLRs) of free and bound water are plotted against FMC in Figure 7. For a moisture content of 70%, the peak mass loss rate of free water was larger than that of bound water approximately by a factor of 1.25. It almost linearly increased to 2.0 for FMC of 130%.

In Figure 8, the variation of solid and gas phase temperatures with time is shown at a location close to the ignitor (1.2 cm upwind of the ignitor). The solid and gas phase at this location attained a maximum temperature of 600°C. For an FMC of 130%, it was observed that in the first 30 s, the temperature of the solid fuel increased up to 100°C. At this temperature, the evolution of free water was dominant, which is also evident from Figure 6a. After 30 s, with an increase in temperature (>200°C), bound water and pyrolysates were released. To better understand the evaporation of free and bound water as function of temperature, Figure 9 is plotted for the single fuel element located 1.2 cm upwind of the ignitor. From this figure, it was observed that at temperatures close to 200°C around time 40 s, free water evaporation is completed and bound water evaporation was initiated.

The variation of heat release rate with time is shown in Figure 10. The peak value of heat release rate (HRR) decreased with an increase in moisture content, owing to the fact that the dry mass of the fuel decreased with an increase in FMC. The case with 70% FMC had a peak HRR of 2.0 kW while the 130% FMC had a peak HRR of 1.3 kW. The ignition times, discussed earlier, were determined using the peak values of HRR. Also, the peak values were observed close to 5 s after the time instant at which ignition was defined.

In Figure 11, distribution of gas phase temperatures on an *xy* slice plane located at $z = 0$ are shown at two different times: 130 s and 135 s for 130% FMC. The heat received from the radiant heater caused the fuel particles to release volatiles, which due to the effect of air flow, was convected over the ignitor located at the downstream location, thereby initiating gas-phase ignition. Hence, the fuel particles located close to the ignitor were subjected to high temperatures and burned faster than fuel elements

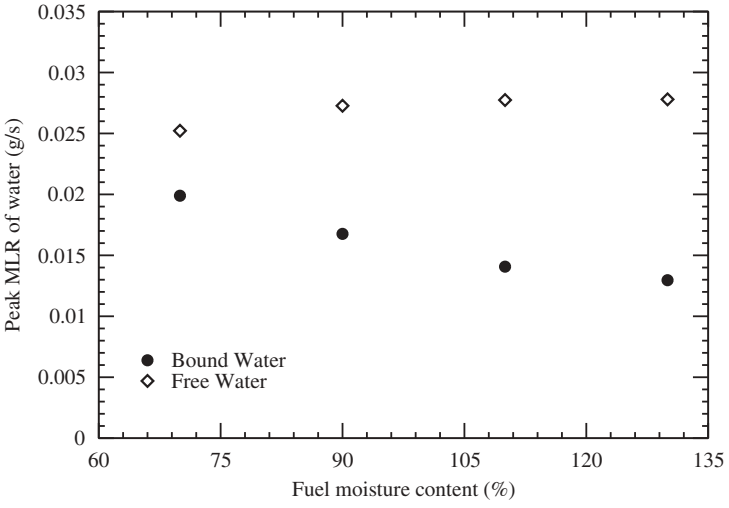


**Figure 7.** Variation of peak mass loss rate of free and bound water against fuel moisture content.

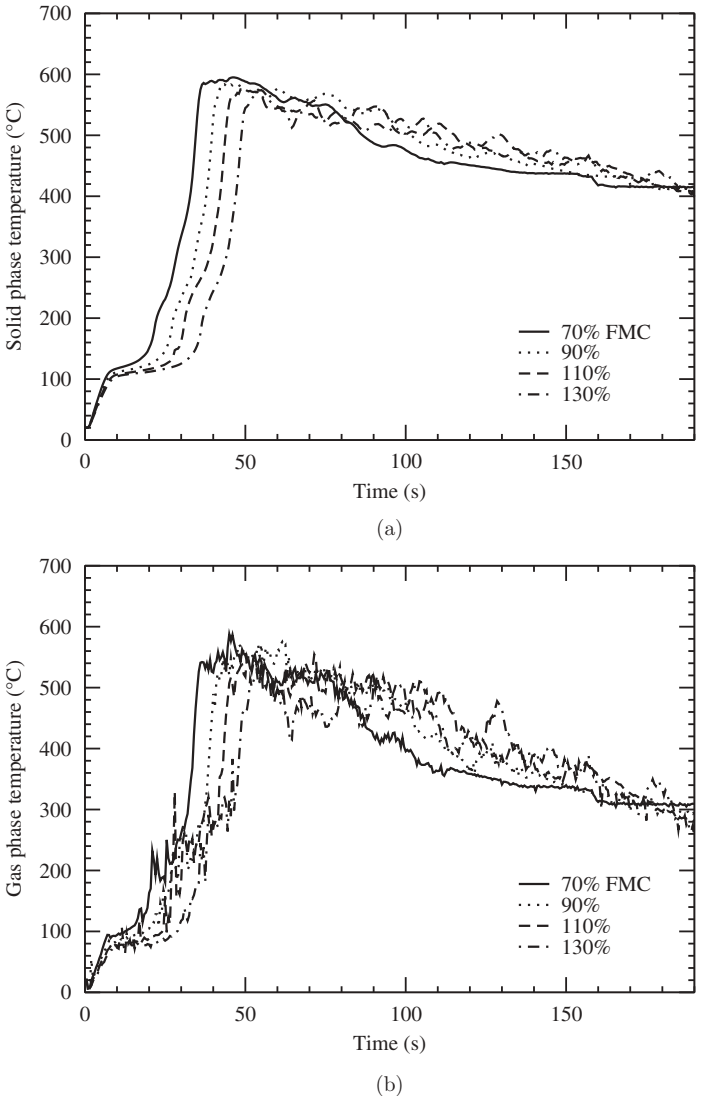


**Figure 8.** Time histories of temperature of (a) solid fuel and (b) surrounding gas phase, at a point located 1.2 cm upwind of the ignitor.

away from it. As time progressed, the rest of the fuel elements burned in a pattern opposite to the direction of wind as observed in the case of a backing-like fire.

In Figure 12, vertically oriented slice planes with contour plots of moisture mass fraction and gas phase temperatures are plotted at time 130 s for 130% FMC. At this time instant, which was well beyond the ignition and peak mass loss time instants, high mass fractions of moisture was observed at locations close to the solid fuel. The gas phase temperatures in this region were observed to be well above 800°C, thereby establishing the behavior of release of moisture in live fuels beyond the time to ignition.

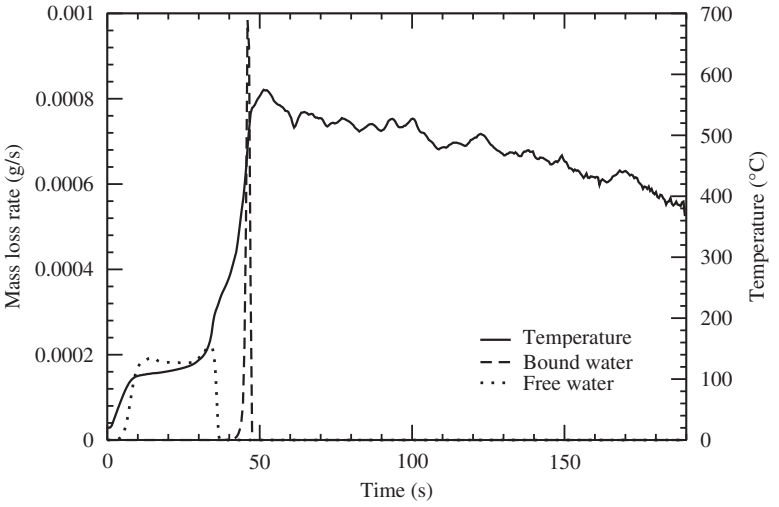


**Figure 9.** Temporal variation of mass loss rate of free and bound water along with the associated solid phase temperature for a fuel element located 1.2 cm upwind of the ignitor.

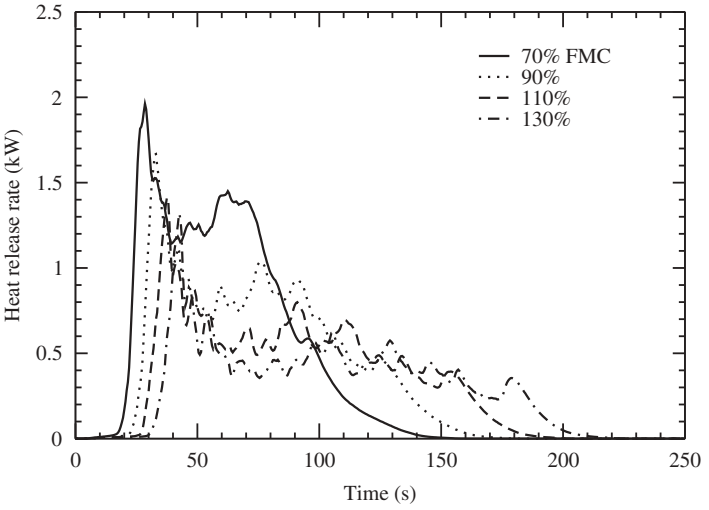


**Figure 10.** Variation of heat release rate with time for various fuel moisture contents.

## Conclusions

A computational study was performed to support the piloted ignition experiments on live Douglas-fir needles in the FIST apparatus. A particle-based approach was used to model the burning of the needles wherein the particles were assumed thermally thin. The fuel moisture content was assumed to be in both free and bound states. The evaporation of free and bound water was modeled by Arrhenius-type rate equations. Hence, the fuel was assumed to undergo a three-stage decomposition process, including evaporation of free water and bound water, pyrolysis, and char oxidation. There was a difference of around 5 s between

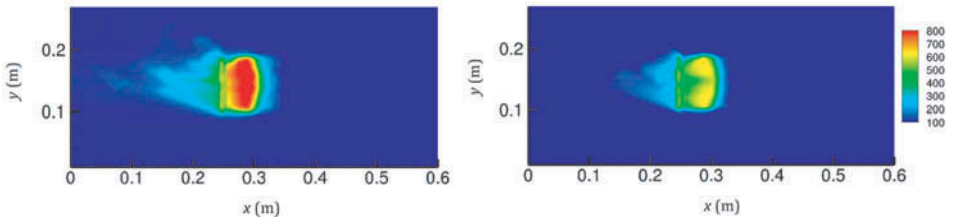


(a) (b)

**Figure 11.** Temperature contours (in °C) of gas phase at a horizontal slice plane passed at $z = 0$ cm (top view) for fuel with 130% FMC at (a) $t = 130$ s and (b) $t = 135$ s.

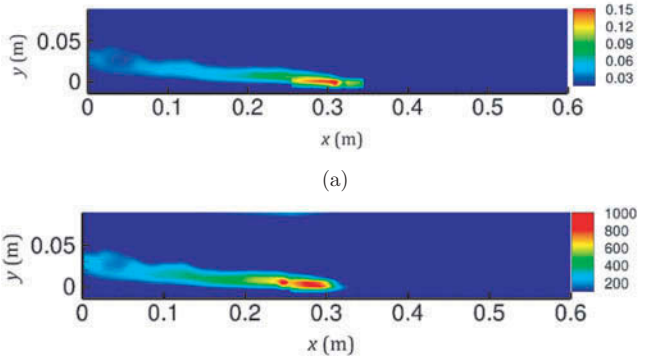


(a)

(b)

**Figure 12.** Color contours at a vertical slice plane passing through $y = 13$ cm (mid-section of the domain) at time instant $t = 130$ s for fuel with 130% FMC: (a) moisture mass fraction contours and (b) gas phase temperature contours (in °C).

the simulated and experimental ignition times at FMC 70% when the bound water was accounted for in the simulation. However, for higher FMC, the simulated ignition times were within the uncertainty of the experimental values. This difference could be attributed to the seasonal effects on needles or evaporation of water by the rupture of cell walls observed in experiments. Neither effect was taken into account in simulations. The mass loss rates obtained by modeling were in good agreement with those obtained by experiments. The relative error between the simulated and modeled maximum peaks was within 5%. It was also observed that free water evaporated at temperatures close to boiling point of water, whereas bound water and volatiles released later at temperatures close to 200°C. Simulations showed that a significant amount of bound water remained in the fuel when ignition occurred.

## Acknowledgments

This work was supported in part by Joint Fire Sciences Program project 11-1-4-19 administered by the USDA Forest Service PSW Research Station through cooperative agreement 11-JV-11272167-103. High performance computing resources and technical support from the Alabama Supercomputer Authority are appreciated.

## ORCID

D. R. Weise http://orcid.org/0000-0002-9671-7203

## References

Albini, F.A. 1980. Thermochemical properties of flame gases from fine wildland fuels. Forest Service Research Paper INT-243. USDA, Ogden, UT.

Atreya, A., and Abu-Zaid, M. 1991. Effect of environmental variables on piloted ignition. *Fire Saf. Sci*., **3**, 177–186.

Babrauskas, V. 2003. *Ignition Handbook*, Fire Science Publishers, Issaquah, WA.

Blackmarr, W.H., and Flanner, W.B. 1968. Seasonal and diurnal variation in moisture content of six species of pocosin shrubs. Forest Service Research Paper SE-33. USDA, Asheville, NC.

Bryden, K.M., Ragland, K.W., and Rutland, C.J. 2002. Modeling thermally thick pyrolysis of wood. *Biomass Bioenergy* **22**(1), 41–53.

Chan, W.-C.R., Kelbon, M., and Krieger, B.B. 1985. Modelling and experimental verification of physical and chemical processes during pyrolysis of a large biomass particle. *Fuel,* **64**(11), 1505–1513.

Deardorff, J.W. 1980. Stratocumulus-capped mixed layers derived from a three-dimensional model. *Boundary Layer Meteorol.,* **18**(4), 495–527.

Dimitrakopoulos, A.and Papaioannou, K.K. 2001. Flammability assessment of mediterranean forest fuels. *Fire Technol,* **37**(2), 143–152.

Dreisbach, J., and Hill, K. 2007. Verification and validation of selected fire models for nuclear power plant applications. NUREG-1824. United States Nuclear Regulatory Commission, Washington, DC.

Ferguson, S.C., Dahale, A., Shotorban, B., Mahalingam, S., and Weise, D.R., 2013. The role of moisture on combustion of pyrolysis gases in wildland fires. *Combust. Sci. Technol*., **185**, 435–453.

Finney, M.A., Cohen, J.D., McAllister, S.S., and Jolly, W.M. 2013. On the need for a theory of wildland fire spread. *Inte. J. Wildland Fire,* **22**(1), 25–36.

Fletcher, T.H., Pickett, B.M., Smith, S.G., Spittle, G.S., Woodhouse, M.M., Haake, E., and Weise, D.R. 2007. Effects of moisture on ignition behavior of moist california chaparral and utah leaves. *Combust. Sci .Technol*, **179**(6), 1183–1203.

Gallacher, J.R. 2016. The influence of season, heating mode and slope angle on wildland fire behavior. PhD thesis. Brigham Young University, Provo, UT.

Grishin, A.M. 1997. *Mathematical Modelling of Forest Fires and New Methods of Fighting Them*, Publishing House of Tomsk State University, Tomsk, Russia.

Jameson, D.A. 1966. Diurnal and seasonal fluctuations in moisture content of pinyon and juniper. Forest Service Research Paper RM-67. USDA, Fort Collins, CO.

Janssens, M. 1991. Fundamental thermophysical characteristics of wood and their role in enclosure fire growth. PhD thesis. Ghent University, Ghent, Belgium.

Jolly, W.M., Hadlow, A.M., and Huguet, K. 2014. De-coupling seasonal changes in water content and dry matter to predict live conifer foliar moisture content. *Int. J. Wildland Fire*, **23**(4), 480.

Jolly, W. M., Parsons, R.A., Hadlow, A.M., Cohn, G.M., McAllister, S.S., Popp, J.B., Hubbard, R.M., Negron, J.F. 2012. Relationships between moisture, chemistry, and ignition of pinus contorta needles during the early stages of mountain pine beetle attack. For. *Ecol. Manage*., **269**, 52–59.

Killebrew, J.B. 1878. *The Grasses of Tennessee: Including Cereals and Forage Plants*, American Company, Nashville, TN.

Kozlowski, T.T., and Clausen, J.J. 1965. Changes in moisture contents and dry weights of buds and leaves of forest trees. *Botanical Gazette*, (126), 20–26.

Little, C. 1970. Seasonal changes in carbohydrate and moisture content in needles of balsam fir (*abies balsamea*). *Cana. J. Bot*., **48**(11), 2021–2028.

McAllister, S., Grenfell, I., Hadlow, A., Jolly, W., Finney, M., and Cohen, J. 2012. Piloted ignition of live forest fuels. *Fire Saf. J*., 51, 133–142.

McGrattan, K., Hostikka, S., McDermott, R., Floyd, J., Weinschenk, C., and Overholt, K. 2013. *Fire Dynamics Simulator,Technical Reference Guide, Volume 1: Mathematical Model*. NIST-SP-1018. National Institute of Standards and Technology, Gaithersburg, MD.

Mell, W., Maranghides, A., McDermott, R., and Manzello, S.L. 2009. Numerical simulation and experiments of burning douglas fir trees. *Combust. Flame,* **156**(10), 2023–2041.

Moghtaderi, B., and Fletcher, D. 1988. Flaming combustion characteristics of wood-based materials. *Fire Saf. Sci*., **3**, 209–220.

Nelson, R.M. 2001. *Water Relations of Forest Fuels*, Academic Press, San Francisco, CA.

Overholt, K.J., Weinschenk, C.G., and Madrzykowski, D. 2014. Simulation of a fire in a hillside residential structure—San Francisco, CA. NIST Technical Note 1856. U.S. Department of Commerce, National Institute of Standards and Technology, Gaithersburg, MD.

Pellizzaro, G., Duce, P., Ventura, A., and Zara, P. 2007. Seasonal variations of live moisture content and ignitability in shrubs of the mediterranean basin. **16**(5), 633–641.

Philpot, C.W. 1965. Diurnal fluctuation in moisture content of ponderosa pine and whiteleaf manzanita leaves. Forest Service Research Paper PSW-67, USDA, Berkeley, CA.

Pickett, B.M., Isackson, C., Wunder, R., Fletcher, T.H., Butler, B.W., and Weise, D.R. 2010. Experimental measurements during combustion of moist individual foliage samples. *Int. J. of Wildland Fire*, **19**, 153–162.

Pope, S.B. 2004. Ten questions concerning the large-eddy simulation of turbulent flows. *New J. Phys*., **6**(1), 35.

Porterie, B., Consalvi, J., Kaiss, A., and Loraud, J. 2005. Predicting wildland fire behavior and emissions using a fine-scale physical model. *Numeri. Heat Transfer*, **47**(6), 571–591.

Prince, D.R. 2014. Measurement and modeling of fire behavior in leaves and sparse shrubs. PhD thesis, Brigham Young University, Provo, UT.

Prince, D.R., and Fletcher, T.H. 2013. A combined experimental and theoretical study of the combustion of live vs. dead leaves. Presented at the 8th US National Combustion Meeting of the Combustion Institute, Park City, UT, May 19–22.

Ross, R.J. 2010. Wood handbook. General Technical Report FPLGTR190. Forest Products Laboratory, USDA Forest Service, Madison, WI.

Rothermel, R. 1972. A mathematical model for predicting fire spread in wildland fuels. Research Paper INT-115, U.S. Department of Agriculture, Intermountain Forest and Range Experiment Station, Ogden, UT.

Simms, D.L., and Law, M. 1967. The ignition of wet and dry wood by radiation. *Combust. Flame*, **11** (5), 377–388.

Smith, S.G., 2005. Effects of moisture on combustion characteristics of live california chaparral and Utah foliageMaster's thesis, Brigham Young University–Provo, Provo, UT.

Van Wagner, C. 1967. Seasonal variation in moisture content of eastern Canadian tree foliage and the possible effect on crown fires. Forestry Branch Canada, Ottawa, Canada.

Wang, X., Fleischmann, C., and Spearpoint, M. 2016. Assessing the influence of fuel geometrical shape on fire dynamics simulator (FDS) predictions for a large-scale heavy goods vehicle tunnel fire experiment. *Case Stud. Fire Saf*., **5**, 34–41.

Weise, D.R., White, R.H., Beall, F.C., and Etlinger, M. 2005. Use of the cone calorimeter to detect seasonal differences in selected combustion characteristics of ornamental vegetation. *Int. J. of Wildland Fire*, **14**(3), 321–338.

Weise, D.R., Zhou, X., Mahalingam, S., and Chong, J. 2015. Marginal fire spread in live fuel beds-horizontal fuels. Forest Service Research Data Archive, Fort Collins, CO.

Xanthopoulos, G., and Wakimoto, R.H. 1993. A time to ignition-temperature-moisture relationship for branches of three western conifers. *Can. J. For. Res*. **23**(2), 253–258.

Yashwanth, B., Gallacher, J., Shotorban, B., Mahalingam, S., Fletcher, T., and Weise, D. 2015. Experimental and numerical investigation of the effect of heating modes and moisture content on pyrolysis and ignition of live fuels. Presented at the 9th US National Meeting, Central States Section of the Combustion Institute, Cincinnati, OH, May 17–20.

## Appendix

&HEAD CHID='Douglas_Fir_Needles_FMC130', TITLE='Mcallister et al. (2012) Wind Tunnel Setup' /

-2 grids(test)
MESH IJK=120,52,21, XB= 0.0,0.3, 0.01,0.27, -0.015,0.09 /
MESH IJK=120,52,21, XB= 0.3,0.6, 0.01,0.27, -0.015,0.09 /

-40 grids

&MESH IJK=3,52,21, XB= 0.00,0.015, 0.01,0.27, -0.015,0.09 /
&MESH IJK=3,52,21, XB= 0.015,0.03, 0.01,0.27, -0.015,0.09 /

&MESH IJK=3,52,21, XB= 0.03,0.045, 0.01,0.27, -0.015,0.09 /
&MESH IJK=3,52,21, XB= 0.045,0.06, 0.01,0.27, -0.015,0.09 /

&MESH IJK=3,52,21, XB= 0.06,0.075, 0.01,0.27, -0.015,0.09 /
&MESH IJK=3,52,21, XB= 0.075,0.09, 0.01,0.27, -0.015,0.09 /

&MESH IJK=3,52,21, XB= 0.09,0.105, 0.01,0.27, -0.015,0.09 /
&MESH IJK=3,52,21, XB= 0.105,0.12, 0.01,0.27, -0.015,0.09 /

&MESH IJK=3,52,21, XB= 0.12,0.135, 0.01,0.27, -0.015,0.09 /
&MESH IJK=3,52,21, XB= 0.135,0.15, 0.01,0.27, -0.015,0.09 /

&MESH IJK=3,52,21, XB= 0.15,0.165, 0.01,0.27, -0.015,0.09 /
&MESH IJK=3,52,21, XB= 0.165,0.18, 0.01,0.27, -0.015,0.09 /

&MESH IJK=3,52,21, XB= 0.18,0.195, 0.01,0.27, -0.015,0.09 /
&MESH IJK=3,52,21, XB= 0.195,0.21, 0.01,0.27, -0.015,0.09 /

&MESH IJK=3,52,21, XB= 0.21,0.225, 0.01,0.27, -0.015,0.09 /
&MESH IJK=3,52,21, XB= 0.225,0.24, 0.01,0.27, -0.015,0.09 /

&MESH IJK=3,52,21, XB= 0.24,0.255, 0.01,0.27, -0.015,0.09 /
&MESH IJK=3,52,21, XB= 0.255,0.27, 0.01,0.27, -0.015,0.09 /

&MESH IJK=3,52,21, XB= 0.27,0.285, 0.01,0.27, -0.015,0.09 /
&MESH IJK=3,52,21, XB= 0.285,0.3, 0.01,0.27, -0.015,0.09 /

&MESH IJK=3,52,21, XB= 0.3,0.315, 0.01,0.27, -0.015,0.09 /
&MESH IJK=3,52,21, XB= 0.315,0.33, 0.01,0.27, -0.015,0.09 /

&MESH IJK=3,52,21, XB= 0.33,0.345, 0.01,0.27, -0.015,0.09 /
&MESH IJK=3,52,21, XB= 0.345,0.36, 0.01,0.27, -0.015,0.09 /

&MESH IJK=3,52,21, XB= 0.36,0.375, 0.01,0.27, -0.015,0.09 /
&MESH IJK=3,52,21, XB= 0.375,0.39, 0.01,0.27, -0.015,0.09 /

&MESH IJK=3,52,21, XB= 0.39,0.405, 0.01,0.27, -0.015,0.09 /
&MESH IJK=3,52,21, XB= 0.405,0.42, 0.01,0.27, -0.015,0.09 /

&MESH IJK=3,52,21, XB= 0.42,0.435, 0.01,0.27, -0.015,0.09 /
&MESH IJK=3,52,21, XB= 0.435,0.45, 0.01,0.27, -0.015,0.09 /

&MESH IJK=3,52,21, XB= 0.45,0.465, 0.01,0.27, -0.015,0.09 /
&MESH IJK=3,52,21, XB= 0.465,0.48, 0.01,0.27, -0.015,0.09 /

```
&MESH IJK=3,52,21, XB= 0.48,0.495, 0.01,0.27, -0.015,0.09 /
&MESH IJK=3,52,21, XB= 0.495,0.51, 0.01,0.27, -0.015,0.09 /

&MESH IJK=3,52,21, XB= 0.51,0.525, 0.01,0.27, -0.015,0.09 /
&MESH IJK=3,52,21, XB= 0.525,0.54, 0.01,0.27, -0.015,0.09 /

&MESH IJK=3,52,21, XB= 0.54,0.555, 0.01,0.27, -0.015,0.09 /
&MESH IJK=3,52,21, XB= 0.555,0.57, 0.01,0.27, -0.015,0.09 /

&MESH IJK=3,52,21, XB= 0.57,0.585, 0.01,0.27, -0.015,0.09 /
&MESH IJK=3,52,21, XB= 0.585,0.60, 0.01,0.27, -0.015,0.09 /

&REAC ID='WOOD'
   FUEL='METHANE'
   SOOT_YIELD = 0.02
   C                = 1.0
   H                = 4.0
   HEAT_OF_COMBUSTION = 55500. /

&TIME T_END=250. /

-Glass Walls
&OBST XB = 0.0,0.6, 0.01,0.01, 0.0,0.09, COLOR = 'GRAY', TRANSPARENCY = 0.5 /
&OBST XB = 0.0,0.6, 0.27,0.27, 0.0,0.09, COLOR = 'GRAY', TRANSPARENCY = 0.5 /

-Metal Wall Top

&OBST XB = 0.0,0.6, 0.01,0.1, 0.09,0.09, COLOR = 'SILVER', TRANSPARENCY = 1.0 /FRONT
&OBST XB = 0.0,0.6, 0.19,0.27, 0.09,0.09, COLOR = 'SILVER', TRANSPARENCY = 1.0 /BACK
&OBST XB = 0.0,0.255, 0.1,0.19, 0.09,0.09, COLOR = 'SILVER', TRANSPARENCY = 1.0 /LEFT
&OBST XB = 0.345,0.6, 0.1,0.19, 0.09,0.09, COLOR = 'SILVER', TRANSPARENCY = 1.0 /RIGHT

-Metal Wall Bottom
&OBST XB = 0.0,0.6, 0.01,0.1, 0.0,0.0, COLOR = 'SILVER', TRANSPARENCY = 1.0 /FRONT
&OBST XB = 0.0,0.6, 0.19,0.27, 0.0,0.0, COLOR = 'SILVER', TRANSPARENCY = 1.0 /BACK OBST
XB = 0.0,0.255, 0.1,0.19, 0.0,0.0, COLOR = 'SILVER', TRANSPARENCY = 1.0 /LEFT
&OBST XB = 0.345,0.6, 0.1,0.19, 0.0,0.0, COLOR = 'SILVER', TRANSPARENCY = 1.0 /RIGHT

-Mass Balance
&OBST XB = 0.255,0.345, 0.1,0.19, -0.007,-0.007, COLOR = 'SILVER', TRANSPARENCY = 1.0
/Bottom
&OBST XB = 0.255,0.255, 0.1,0.19, -0.007, 0.0, COLOR = 'SILVER', TRANSPARENCY = 1.0 /Left
&OBST XB = 0.345,0.345, 0.1,0.19, -0.007, 0.0, COLOR = 'SILVER', TRANSPARENCY = 1.0 /Right
&OBST XB = 0.255,0.345, 0.1,0.1, -0.007, 0.0, COLOR = 'SILVER', TRANSPARENCY = 1.0 /Front
&OBST XB = 0.255,0.345, 0.19,0.19, -0.007, 0.0, COLOR = 'SILVER', TRANSPARENCY = 1.0 /Back

-Vent Air Inlet = 1.0 m/s
&SURF ID = 'AIR INLET', VEL = -1.0 /

&VENT SURF_ID     = 'AIR INLET',
   COLOR          = 'GRAY',
   TRANSPARENCY = 0.5,
   XB             = 0.6,0.6,0.01,0.27,0.0,0.09/
   -Specify Heat Release Rate
   SURF ID        = 'FIRE',
   TMP_FRONT      = 698.0/
   *————————————————————————————————————*
```

```
- Ignitor particles
&PART ID = 'IGNITOR ELEMENTS',
   TREE                                = .TRUE.,
   QUANTITIES                          = 'VEG_TEMPERATURE',
   VEG_INITIAL_TEMPERATURE             = 1500.,
   VEG_SV                              = 8366.,
   VEG_DRAG_COEFFICIENT                = 0.1,
   VEG_DENSITY                         = 1., VEG_BULK_DENSITY = 1. /

&TREE PART_ID                          = 'IGNITOR ELEMENTS',
   FUEL_GEOM                           = 'RECTANGLE',
   IGNITOR_ELEMENTS                    = .TRUE.,
   TON_IGNITOR_ELEMENTS                = 0.5,
   T_RAMPON_IGNITOR_ELEMENTS           = 1.0,
   TOFF_IGNITOR_ELEMENTS = 500.,
   T_RAMPOFF_IGNITOR_ELEMENTS = 0.5,
   XB = 0.243,0.2505,0.1,0.19,0.000,0.005/

-Tree vegetation
&PART ID                               = 'needles',
   TREE                                = .TRUE.,
   QUANTITIES                          = 'VEG_TEMPERATURE',
   VEG_INITIAL_TEMPERATURE             = 20.,
   VEG_SV                              = 8366.,
   VEG_MOISTURE                        = 1.3,
   VEG_CHAR_FRACTION                   = 0.25,
   VEG_DRAG_COEFFICIENT                = 0.375,
   VEG_DENSITY                         = 550.,
   VEG_BULK_DENSITY                    = 42.9,
   VEG_DEGRADATION                     = 'ARRHENIUS',
   VEG_CHAR_OXIDATION                  = .TRUE.,
   VEG_REMOVE_CHARRED                  = .TRUE. /

&TREE PART_ID                          = 'needles',
   FUEL_GEOM                           = 'RECTANGLE',
   OUTPUT_TREE                         = .TRUE.,
   LABEL                               = 'needles',
   XB = 0.255,0.345,0.1,0.19,-0.005,0.0 /
   *————————————————————————————————*
&SPEC ID                               = 'WATER VAPOR' /
&SPEC ID                               = 'OXYGEN' /
&SPEC ID                               = 'CARBON DIOXIDE' /

&VENT MB                               = XMIN, SURF_ID = 'OPEN' /
&VENT MB                               = YMIN, SURF_ID = 'OPEN' /
&VENT MB                               = YMAX, SURF_ID = 'OPEN' /
&VENT XB                               = 0.6,0.6,0.0,0.3,-0.015,0.0, SURF_ID = 'OPEN' /

–UP
&VENT XB = 0.255,0.345, 0.1,0.19, 0.09,0.09, SURF_ID = 'FIRE'/
VENT XB = 0.0,0.6, 0.0,0.1, 0.09,0.09, SURF_ID = 'OPEN'/FRONT
VENT XB = 0.0,0.6, 0.19,0.3, 0.09,0.09, SURF_ID = 'OPEN'/BACK
VENT XB = 0.0,0.255, 0.1,0.19, 0.09,0.09, SURF_ID = 'OPEN'/LEFT_MID
VENT XB = 0.345,0.6, 0.1,0.19, 0.09,0.09, SURF_ID = 'OPEN'/RIGHT_MID
```

```
&DUMP DT_SLCF = 2,
   DT_PART = 1 /

&DUMP PLOT3D_QUANTITY(1) = 'MASS FRACTION', PLOT3D_SPEC_ID(1) = 'METHANE' /
&DUMP PLOT3D_QUANTITY(2) = 'MASS FRACTION', PLOT3D_SPEC_ID(2) = 'WATER
VAPOR' /
&DUMP PLOT3D_QUANTITY(3) = 'MASS FRACTION', PLOT3D_SPEC_ID(2) = 'OXYGEN' /
&DUMP PLOT3D_QUANTITY(4:5) = 'TEMPERATURE', 'VELOCITY', DT_PL3D = 5.0,
WRITE_XYZ = .TRUE./

&SLCF PBY = 0.13, QUANTITY='TEMPERATURE', VECTOR=.TRUE. /
&SLCF PBY = 0.13, QUANTITY='VELOCITY', VECTOR=.TRUE. /
&SLCF PBY = 0.13, QUANTITY='HRRPUV' /
&SLCF PBY = 0.13, QUANTITY='MASS FRACTION', SPEC_ID='METHANE' /
&SLCF PBY = 0.13, QUANTITY='MASS FRACTION', SPEC_ID='OXYGEN' /
&SLCF PBY = 0.13, QUANTITY='MASS FRACTION', SPEC_ID='CARBON DIOXIDE' /
&SLCF PBY = 0.13, QUANTITY='MASS FRACTION', SPEC_ID='WATER VAPOR' /
&SLCF PBZ = 0.0025, QUANTITY='TEMPERATURE', VECTOR=.TRUE. /
&SLCF PBZ = 0.0025, QUANTITY='VELOCITY', VECTOR=.TRUE. /

&SLCF PBZ = 0.0025, QUANTITY='HRRPUV' /
&SLCF PBZ = 0.0025, QUANTITY='MASS FRACTION', SPEC_ID='METHANE' /
&SLCF PBZ = 0.0025, QUANTITY='MASS FRACTION', SPEC_ID='OXYGEN' /
&SLCF PBZ = 0.0025, QUANTITY='MASS FRACTION', SPEC_ID='CARBON DIOXIDE' /
&SLCF PBZ = 0.0025, QUANTITY='MASS FRACTION', SPEC_ID='WATER VAPOR' /

&SLCF PBZ = 0.00, QUANTITY='TEMPERATURE', VECTOR=.TRUE. /
&SLCF PBZ = 0.00, QUANTITY='VELOCITY', VECTOR=.TRUE. /
&SLCF PBZ = 0.00, QUANTITY='HRRPUV' /
&SLCF PBZ = 0.00, QUANTITY='MASS FRACTION', SPEC_ID='METHANE' /
&SLCF PBZ = 0.00, QUANTITY='MASS FRACTION', SPEC_ID='OXYGEN' /
&SLCF PBZ = 0.00, QUANTITY='MASS FRACTION', SPEC_ID='CARBON DIOXIDE' /
&SLCF PBZ = 0.00, QUANTITY='MASS FRACTION', SPEC_ID='WATER VAPOR' /

&TAIL /
```